DOI: 10.13009/EUCASS2019-418

DOI: ADD DOINUMBER HERE

Investigation of Flashing LN2-Jets in Terms of Spray Morphology, Droplet Size and Velocity Distributions

Andreas Rees[⋆†], *Heiko Salzmann*[⋆], *Joachim Sender*[⋆] *and Michael Oschwald*[⋆]
[⋆]*German Aerospace Center (DLR), Institute of Space Propulsion*
D-74239 Hardthausen, Germany
andreas.rees@dlr.de ·
[†]Corresponding author

Abstract

For a detailed experimental investigation of superheated cryogenic fluids the new cryogenic test bench M3.3 with a temperature controlled injection system was built at the DLR Institute of Space Propulsion in Lampoldshausen. In a first test campaign flash boiling liquid nitrogen sprays were visualized by means of high-speed shadowgraphy to determine the resulting spray patterns and spray angles. The cryogenic spray patterns are compared with break-up correlations for storable fluids from literature. The dependence of droplet velocities and diameters on the injection conditions was investigated at a constant position in the spray by means of Phase Doppler Anemometry.

Nomenclature

χ	onset criterion [-]
ΔT^*	degree of superheat [-]
Φ	correction factor [-]
ρ	density [kg/m^3]
σ	surface tension [N/m]
θ	spray angle [°]
c_p	specific heat [J/(K kg)]
D	diameter [m]
D_{10}	arithmetical mean diameter [µm]
H	height [m]
h_vap	heat of vaporization [J/kg]
Ja	Jakob number [-]
L	length [m]
p	pressure [Pa]
R_p	degree of superheat [-]
T	temperature [K]
U	vertical velocity component [m/s]
u	velocity [m/s]
V	horizonal velocity component [m/s]
We	Weber number [-]

Subscripts

∞	ambient condition
c	chamber condition
g	gaseous
inj	injection condition
l	liquid
lo	lower
sat	saturation condition
up	upper

1. Introduction

Technology development for propulsion systems of upper stages like the cryogenic ESC-A engine HM-7B or the future Ariane 6 upper stage engine Vinci and for future cryogenic thrusters in reaction control or orbital and maneuvering systems is driven by the invention of new, green propellants to substitute hydrazine and by new ignition technologies like laser ignition [10]. At high-altitude conditions prior to ignition the liquid propellants are injected into the combustor

DOI: 10.13009/EUCASS2019-418

at near-vacuum conditions. This means that the ambient pressure p_∞ is lower than the liquid's saturation pressure $p_{sat}(T_{inj})$ at the injection temperature T_{inj}. The sudden pressure drop at injection leads to a superheated liquid in a metastable thermodynamic state. The injection of a liquid like that results in a fast expansion and eruptive evaporation, a process called flash boiling or flash evaporation. The evaporating gases raise the pressure inside the combustion chamber until the equilibrium pressure shortly before ignition is reached. To know the composition related to phase, species and temperature distribution is important for both to determine the probability of a successful ignition and to avoid destructive pressure peaks.

1.1 Flash boiling

The dominating parameters for the flash boiling phenomenon are the injection temperature T_{inj} and the back pressure p_{c}, which can be a near-vacuum chamber pressure or ambient. According to figure 1 they both define the degree of superheat of the injected liquid in terms of the pressure ratio

$$R_{\mathrm{p}} = \frac{p_{\mathrm{sat}}(T_{\mathrm{inj}})}{p_{\mathrm{c}}} \tag{1}$$

or the ratio of temperature differences

$$\Delta T^* = \frac{\Delta T}{\Delta T_{\mathrm{sat}}} = \frac{T_{\mathrm{inj}} - T_{\mathrm{sat}}(p_{\mathrm{c}})}{T_{\mathrm{sat}}(p_{\mathrm{inj}}) - T_{\mathrm{sat}}(p_{\mathrm{c}})} \tag{2}$$

with the chamber pressure p_{c}, the saturation temperature $T_{\mathrm{sat}}(p_{\mathrm{c}})$ at the chamber pressure p_{c} and the saturation temperature $T_{\mathrm{sat}}(p_{\mathrm{inj}})$ at the injection pressure p_{inj}. A superheated liquid jet with a high degree of superheat is atomized close to or already in the injector nozzle due to vaporization and produces a fine spray with a big opening angle and small droplets. The influence of aerodynamical processes on the primary atomization can be neglected in this kind of jets [22]. The vaporization and expansion of a flash boiling spray leads to a cool-down to reach a new equilibrium state at the saturation temperature $T_{\mathrm{sat}}(p_{\mathrm{c}})$.

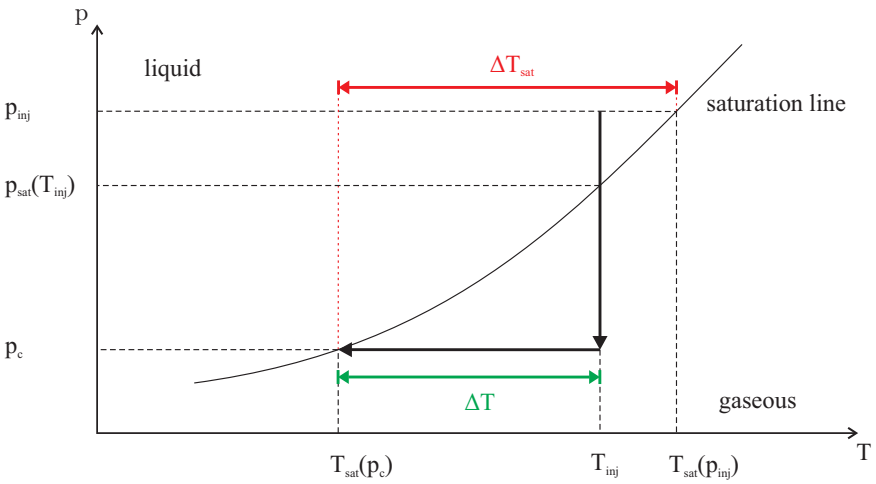

Figure 1: Phase diagram of a superheated liquid for adiabatic depressurization

1.2 State of research

Flash boiling is observed and investigated since the beginning of the 20$^{\mathrm{th}}$ century [11,19]. In the last three decades there have been increased efforts of the automotive industry to investigate flash boiling processes of storable liquids typical for the injection into gasoline or diesel engines [1, 5, 16, 17]. Pre-heating the fuel to reach the superheated condition causes flash boiling during the injection which leads to a finer and wider atomization in the combustion chamber. This increases the efficiency and reduces exhaust emissions [17]. Compared with cavitation in the injector nozzle flash boiling was found to be the dominant process for the fuel atomization [1]. Adding small amounts of low boiling liquids to the actual fuel can be used to improve atomization by flash boiling [5]. First models were developed for flash boiling hydrocarbon sprays to predict the nucleation rates and resulting droplet sizes [16] and for water sprays to predict the

DOI: 10.13009/EUCASS2019-418

liquid superheat with the help of the depressurization transient [4]. Further studies about flash boiling processes can be found concerning the safety field in process technology or chemical and nuclear industry, where storable fluids like hydrocarbons, water, ethanol or refrigerants like R-134A were used [2, 4, 14, 18, 21]. It was found that not only the degree of superheat determines the intensity of flash boiling but also injection conditions like the injection pressure or the injector diameter [21]. By the means of shadowgraphy a remaining liquid core in flash boiling sprays was visualized, where the jet break-up due to phase change takes place in a radial direction [14, 18]. The two correlations

$$Ja\,\Phi = 55\,We_{\mathrm{g}}^{-\frac{1}{7}} \tag{3}$$

for the beginning of the transition region to flashing conditions and

$$Ja\,\Phi = 150\,We_{\mathrm{g}}^{-\frac{1}{7}} \tag{4}$$

for the fully flashing region were empirically developed for superheated water leaking into the atmosphere to subdivide the resulting sprays into an aerodynamical break-up region, a transition region and a fully flashing region [2, 20]. These correlations are only depending on the dimensionless Weber and Jakob numbers

$$We_{\mathrm{g}} = \frac{\rho_{\mathrm{g}} u_{\mathrm{inj}}^2 D_{\mathrm{inj}}}{\sigma_{\mathrm{l}}} \quad \text{and} \quad Ja = \frac{\rho_{\mathrm{l}}}{\rho_{\mathrm{g}}} \frac{c_{\mathrm{p,l}} \Delta T}{h_{\mathrm{vap}}} \tag{5}$$

with the gaseous and liquid densities ρ_{g} and ρ_{l}, the injection velocity u_{inj}, the injector diameter D_{inj}, the liquid's surface tension σ_{l} and specific heat at constant pressure $c_{\mathrm{p,l}}$, the temperature difference $\Delta T = T_{\mathrm{inj}} - T_{\mathrm{sat}}(p_{\mathrm{c}})$ and the heat of vaporization h_{vap} as well as on the correction factor

$$\Phi = 1 - \exp\left[-2300 \frac{\rho_{\mathrm{g}}}{\rho_{\mathrm{l}}}\right]. \tag{6}$$

The validity range of these correlations was successfully expanded for the fluids iso-octane, acetone and ethanol [8]. In the same study the onset criterion χ, which links flash boiling with the classcial nucleation theory, for the flashing regimes was developed and a model for predicting the spray angle in the near-nozzle region by the degree of superheat and the dimensionless surface tension was generated.

In contrast to storable fluids, flash boiling of cryognic liquids is much less investigated due to significantly harder experimental conditions. Within an experimental study at DLR Lampoldshausen about laser ignition in a model rocket combustion chamber at high-altitude conditions flash boiling was observed for a liquid oxygen (LOX) jet [3]. Due to a co-flow by gaseous hydrogen the spray angles however were quite narrow for flash boiling sprays. At the same test bench flash boiling of LOX jets with two injection configurations was investigated and the results were compared to flash boiling sprays of storable fluids [7]. Despite the huge differences in their physical properties the LOX sprays and the sprays with storable liquids showed a similar spray morphology. The used injection system, however, was limited in terms of controlling and adjusting the injection temperature. In another experimental study about cryogenic flash boiling, sprays of liquid nitrogen for injection times of about 10 s were observed with high-speed shadowgraphy for different injection conditions and injector geometries [9]. The resulting sprays showed maximum spray angles of about 140° and the injector geometry and injection pressure did not have big influences on the spray angles. Furthermore a solidification of nitrogen was observed. Temperature measurements along the spray axis yielded a cool down of the sprays below the triple point.

Since the dominating parameters for flash boiling are the injection temperature T_{inj} and the back pressure p_{c}, it is important for an experimental investigation to make them adjustable, to keep them constant during the injection period and to make them reproducible. Especially adjusting and controlling the temperature was partly limited in the few studies with cryogenic flash boiling. This is why the new test bench M3.3 with a temperature controlled injection system was built at DLR Lampoldshausen for a detailed experimental investigation of cryogenic flash boiling processes [12, 13].

2. Experimental set-up

2.1 Test bench M3.3

The test bench M3.3 consists of three main systems, as depicted in figures 2 and 3: the media supply and pressurization system, the cryogenic temperature adjustment and injection system (CTAIS) and the vacuum system. With the

DOI: 10.13009/EUCASS2019-418

first system all gases (nitrogen, helium, oxygen) for the operation of the test bench are provided and pressurized with various pressure reducers to the desired pressures. The second of the three main systems consists of a double-walled and vacuum-insulated pressure tank filled with liquid and gaseous nitrogen (LN2, GN2), see figure 3 on the left and right. By an evacuation or pressurization of the GN2 phase in the pressure tank the fluid is cooled down or heated up, respectively. In the first case a new saturation state is reached due to vaporization of a certain amount of LN2. The latent heat of vaporization necessary for this phase change leads to a loss of heat of the liquid/gaseous nitrogen and consequently to a temperature decrease. In the second case the saturation state after pressurization with GN2 is reached due to condensation of the liquid phase. In this process the latent heat of vaporization is released and heats the nitrogen. Inside the pressure tank is the complete LN2/LOX feed and injection system, which consists of a 0.5 L LN2/LOX run-tank, a mass flowmeter, the injector unit with a pneumatic run valve and the injector nozzle, and piping in-between, see figure 3 in the middle. That means that all these sub-systems are completely surrounded by the cooling medium nitrogen to provide a homogenous temperature distribution from the run-tank to the injector nozzle. Several dynamic pressure and temperature sensors are installed at the nitrogen pressure tank as well as at the feed and injection system, in order to both control and adjust the temperature of the cooling medium and to measure the injection parameters of the injected jets. The latter is realized by a Pt100A temperature sensor and a dynamic pressure sensor 601A by Kistler each installed about 30 mm upstream of the injector nozzle exit. A hand hole at the top of the pressure tank provides the feedthroughs for the sensors and the supply pipes for LN2, GN2 and Helium. The latter is used to pressurize the pneumatic axial run valve (Axius by Stöhr Armaturen) as well as the cable ducts for the sensor cables inside the pressure tank.

The CTAIS is mounted on top of the vacuum system, which is a cylindrical chamber with an inner diameter of 300 mm, a height of 225 mm from the injector nozzle exit to the bottom of the chamber and four optical accesses with a diameter of 100 mm each. An attached vacuum pump with a pumping speed of 87.5 $\frac{m^3}{h}$ produces the near-vacuum atmosphere to simulate high-altitude conditions.

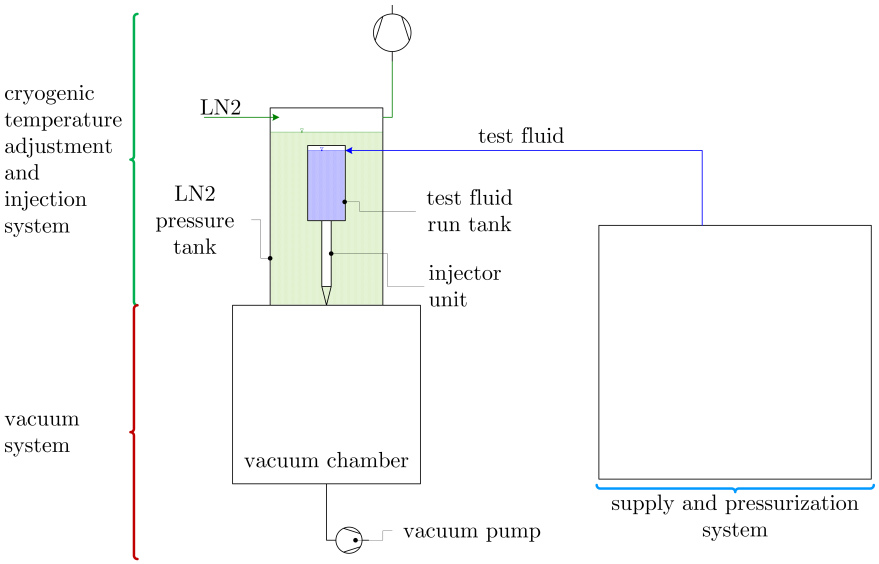

Figure 2: Schematic illustration of the DLR test bench M3.3 with the three main systems

After evacuating all of the pipes and vessels of the CTAIS the system is chilled-down in about 90 minutes by filling it with LN2. During chill-down the run-tank is filled with the gaseous test fluid, which is nitrogen for the current study, and gets liquified when the chill-down is finished.

The CTAIS allows variable injection conditions, which are summarized in table 1. In the first run-in tests it was shown that the system is capable of keeping the injection temperature T_{inj} constant during the whole injection time of about 2 s, that the injection temperature is reproducible in the range of ±0.6 K for each test run and that the temperature distribution is homogeneous in the whole test fluid feed line [12].

DOI: 10.13009/EUCASS2019-418

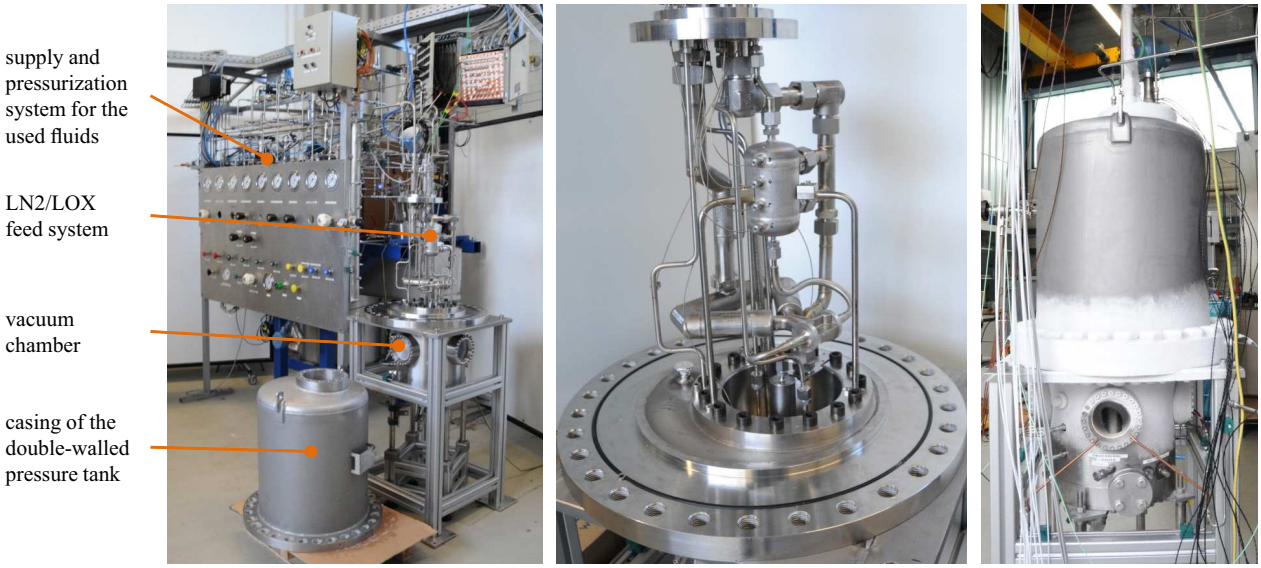

Figure 3: Left: test bench M3.3 with supply and pressurization system, open CTAIS and vacuum system; middle: open CTAIS with run tank, pneumatic run valve, injector unit and sensoric in-between; right: chilled-down test bench M3.3 in operation mode

Table 1: Possible injection conditions of test bench M3.3

parameter	**range**	**unit**
injection temperature T_{inj}	75 - 120	K
injection pressure p_{inj}	1 - 20	10^5 Pa
back pressure p_c	30 - 1000	10^2 Pa
injector diameter D_{inj}	1 - 2	10^{-3} m
mass flow $\dot{m}$	0.08 - 50	g/s

2.2 Optical diagnostics

2.2.1 High-speed shadowgraphy

In a first test campaign high-speed backlight shadowgraphy was used to visualize the injected LN2 sprays. With a xenon light source the sprays were illuminated from the backside through one of the four optical accesses of the vacuum chamber. A translucent milk glas screen was placed between the light source and the chamber window to provide a homogeneous background. The high-speed camera is positioned on the opposite optical access of the chamber. The optical set-up is shown schematically in figure 4 and the used components are listed in table 2. The high-speed camera was set to 10 000 fps with a resolution of 1024 × 1024 pixels.

Table 2: Components of optical shadowgraphy set-up at test bench M3.3

component	**manufacturer**	**type**
xenon light source	Müller Elektrik & Optik	SVX 1450 & LAX 1450
camera lense	Tamron	A061 AF28-300mm
camera	Photron	Fastcam SA-X

To determine the spray angles the resulted shadowgraphs were post-processed by an algorithm, which was used in [7] and adapted to the optical and geometrical set-up of test bench M3.3 [15]. As can be seen in figure 5 the algorithm detects the spray contour and the upper and lower spray angle can be calculated by the trigonometrical relation

$$\theta_{up,lo} = \frac{180°}{\pi} \arctan\left(\frac{H_{up,lo}}{L}\right) \tag{7}$$

DOI: 10.13009/EUCASS2019-418

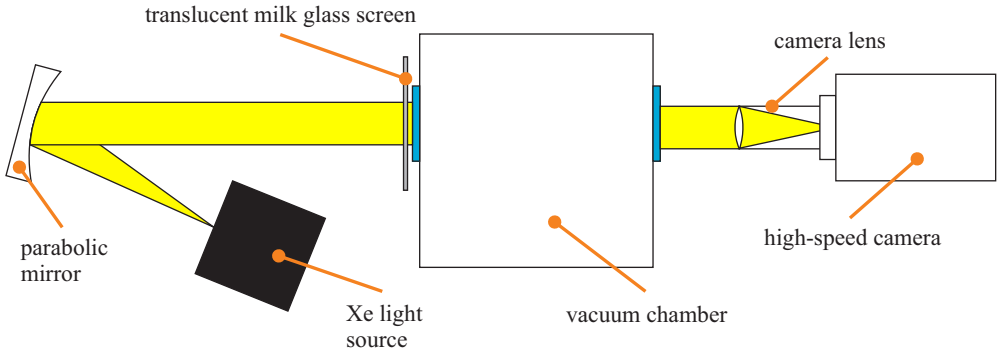

Figure 4: Scheme of the optical set-up for high-speed backlight shadowgraphy at test bench M3.3

with the upper and lower heights H_{up} and H_{lo} and the length L of the spray contour at different L/D-ratios. At an evaluation time of 120 ms after starting the injection 50 images are averaged in a period of 120 ms ± 2.5 ms to calculate an averaged spray angle with an uncertainty of about $\Delta\theta = \pm 3.9°$.

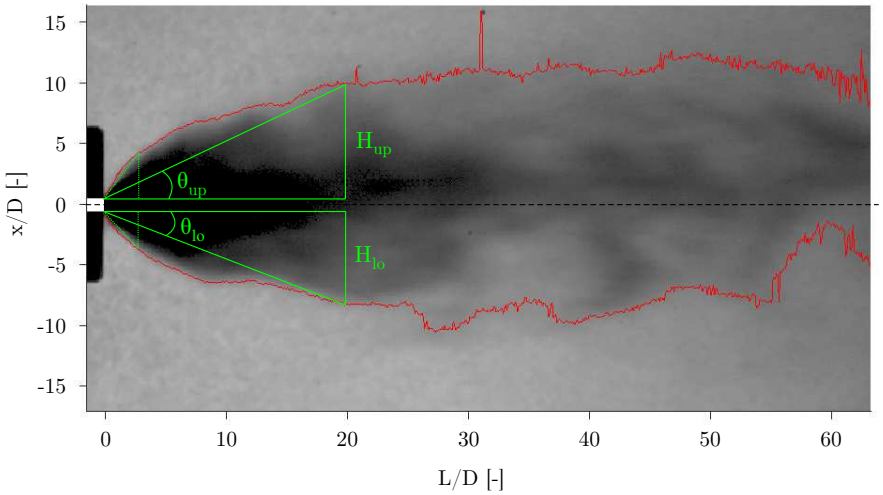

Figure 5: Determination of spray angle θ at different L/D-positions by post-processing shadowgraph images

2.2.2 Phase Doppler Anemometry

For the measurement of the local vertical and horizontal droplet velocity distributions and of the size distributions in flash boiling LN2 sprays a Phase Doppler Anemometry (PDA) system by Dantec Dynamics in the dual-mode configuration was used in a second measurement campaign, see figures 6 and 7. The receiver probe was positioned with an off-axis angle of 12° to use forward scattering first order refraction and a spatial filter with a slit of 200 µm was chosen. The main components of the PDA system are summarized in table 3. The refractive index for nitrogen was set to 1.205 according to an interpolation of values derived from [6] in respect to the current wavelengths and to the temperature range for this measurement campaign.

Table 3: Components of optical PDA set-up at test bench M3.3

component	**specification**
two DopplerPower DPSS lasers	1 W each; 488 nm and 514 nm wavelength
2D transmitter probe	D = 60 mm; 2.2 mm beam diameter
DualPDA receiver probe	D = 112 mm
two front lenses	500 mm focal length; 93 mm aperture
burst processor P800-2D	
2D traverse system	

DOI: 10.13009/EUCASS2019-418

Based on this optical set-up of the PDA system, droplets with a maxium particle diameter of 72 µm can be measured. The velocity ranges were set to $-13\,\text{m/s} \leq U \leq 40\,\text{m/s}$ for the vertical velocity component and to $-10\,\text{m/s} \leq V \leq 10\,\text{m/s}$ for the horizontal one. The reason for the narrow horizontal velocity span is the measurement position on the spray axis where no or only small horizontal velocity vectors are expected. This position at the center of the optical access, i.e. about 48 mm downstream of the injector nozzle exit along the spray axis, was held constant for the whole measurement campaign in the presented study. The statistical errors can be quantified with $\Delta U = \pm 1.5\,\text{m/s}$, $\Delta V = \pm 0.6\,\text{m/s}$ and $\Delta D = \pm 2.4\,\mu\text{m}$. The detected signals are evaluated and arithmetically averaged for a time period of 120 to 220 ms after injection start due to steady state injection conditions in this interval.

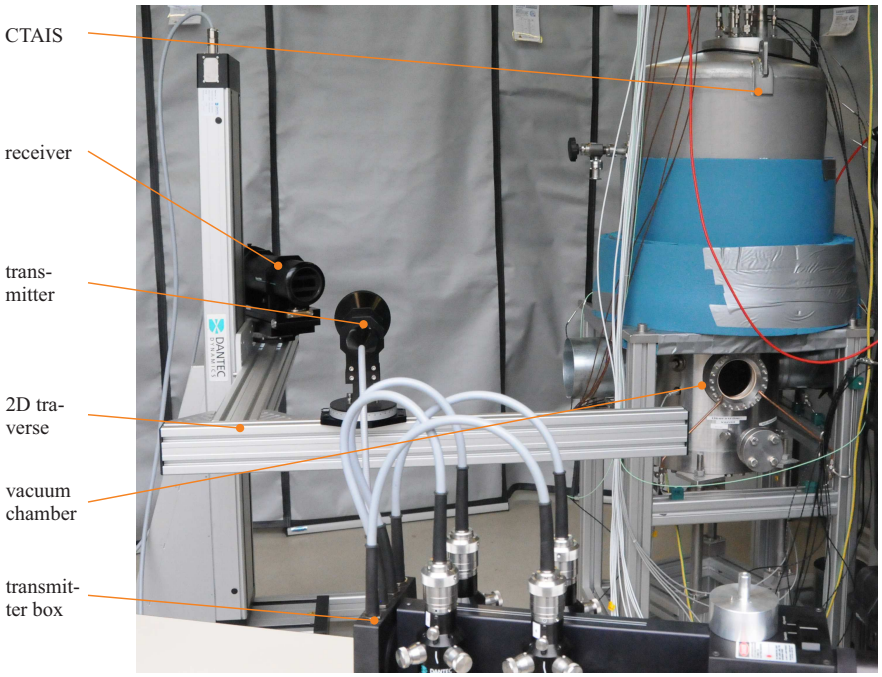

Figure 6: Optical set-up of Dual-Mode PDA system at test bench M3.3

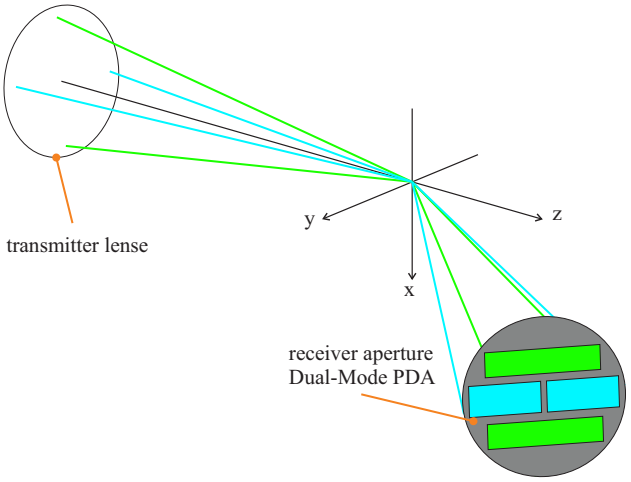

Figure 7: Receiver aperture of the used Dual-Mode PDA system

DOI: 10.13009/EUCASS2019-418

3. Results and discussion

3.1 Shadowgraphy campaign

In a first test series the degree of superheat R_p was increased by a variation of the back pressure p_c from 36 to 600×10^2 Pa to show the spray evolution of flash boiling LN2 sprays. The injection temperature $T_{inj} = 82.5 \pm 0.6$ K and the injection pressure $p_{inj} = 4.0 \pm 0.2 \times 10^5$ Pa were kept constant for all of the test runs depicted in figure 8. An injector with a diameter of $D_{inj} = 1$ mm and an $L/D = 2.9$ was used for all of the jets presented in this paper. Each of the shown shadowgraph images was made 120 ms after the start of the injection. The sprays with lower superheat, i.e. $R_p \approx 3$ show typical features of an aerodynamical break-up like long liquid cores in the spray center line, small opening angles and large liquid filaments. For increasing R_p the LN2 sprays become wider and more turbulent flow structures can be observed until the flash boiling process dominates the jet break-up for a degree of superheat $R_p > 12$. In these fully flashing sprays the remaining liquid core is quite small and exists only at the injector outlet while the remaining liquid structures are monodisperse droplet systems.

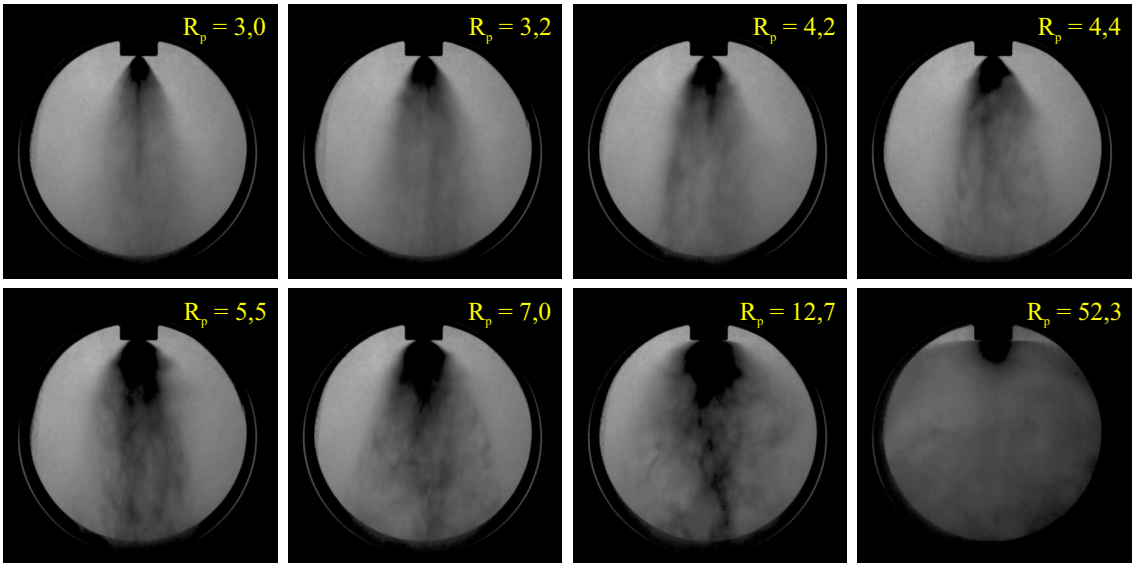

Figure 8: LN2 sprays at different degrees of superheat R_p at $T_{inj} = 82.5$ K, $p_{inj} = 4 \times 10^5$ Pa and $D_{inj} = 1.0$ mm

In figure 9 the influence of the injection pressure p_{inj} is shown, which was increased to $p_{inj} = 8.0 \pm 0.3 \times 10^5$ Pa for the same injection temperature T_{inj}, injector geometry D_{inj} and back pressure range p_c. The opening angles of the resulting sprays are much smaller and larger liquid structures can be seen in the sprays compared to figure 8. For similar degrees of superheat R_p the influence of the flash boiling process onto the spray pattern is smaller for the higher injection pressure.

By calculating the Weber number, the Jakob number and the correction factor Φ according to equations (3), (4) and (6) the 16 LN2 sprays of the figures 8 and 9 are compared with the correlations by Cleary et al. [2]. As can be seen in figure 10 the LN2 sprays fit well into the three regions defined by these correlations although they were developed for storable fluids with quite different physical properties. All of the sprays with typical features of flash boiling sprays and a degree of superheat $R_p \geq 7$ are above the red line, which is defined as the start of the fully flashing regime. Since within this test series the injection conditions led to superheats not smaller than $R_p = 3$, no jets with a pure aerodynamical break-up were generated. Hence there are no data points below the blue line, which represents the end point of the aerodynamical break-up regime. The shift of the test runs with the same injection temperature and pressure towards lower Weber numbers for an increasing product of $\Phi \times Ja$ is due to the dependence of the Weber number on the density of the gaseous phase ρ_g in the vacuum chamber. This gaseous phase is directly linked to the pressure of the chamber atmosphere, i.e. the varied back pressure p_c. In the case of the test runs with the low injection pressure of $p_{inj} = 4 \times 10^5$ Pa the back pressure was in the range of $p_c = 37$ to 600×10^2 Pa, which is an increase by a factor of approximately 16 and consistent with the increase of $\Phi \times Ja$.

DOI: 10.13009/EUCASS2019-418

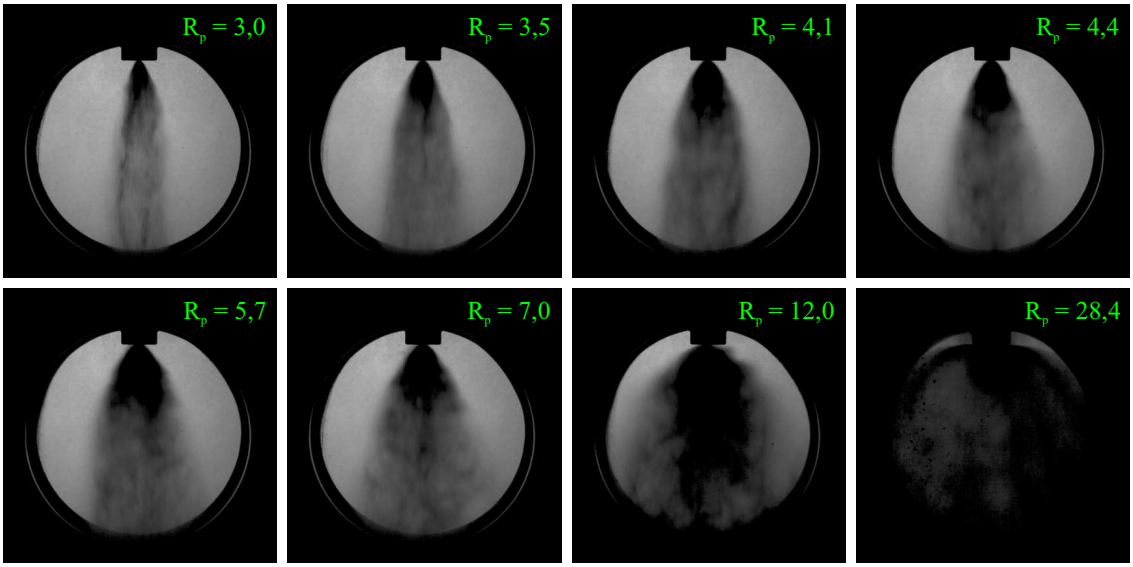

Figure 9: LN2 sprays at different degrees of superheat R_p at $T_{inj} = 82.5$ K, $p_{inj} = 8 \times 10^5$ Pa and $D_{inj} = 1.0$ mm

The sprays with an injection pressure of $p_{inj} = 8 \times 10^5$ Pa are shifted by a factor of about three towards higher Weber numbers compared to the sprays with the lower injection pressure. This is because of the doubling of the injection pressure which leads to a higher mass flow with an increase of the injection velocity u_{inj} by a factor of about 1.8, while all of the other conditions stay constant.

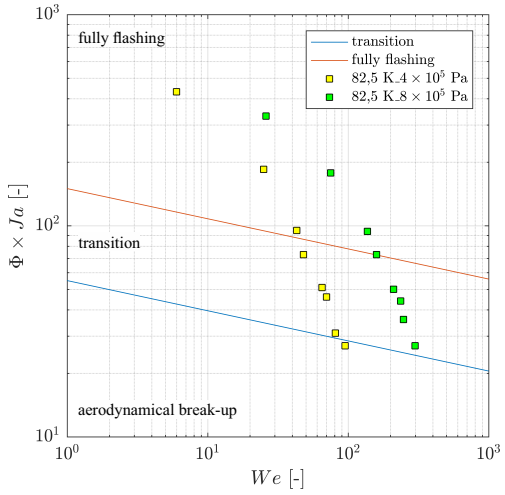

Figure 10: Flashing regimes of LN2 sprays at $T_{inj} = 82.5$ K, $p_{inj} = 4$ and 8×10^5 Pa and $D_{inj} = 1.0$ mm with respect to the correlations of Cleary et al. [2], see equations (3) and (4)

To quantify the visual impression about the relation between the degree of superheat R_p and the opening angles θ of the LN2 sprays from figures 8 and 9, these angles are calculated at different axial positions $L/D = 1; 2; 5; 10; 15$ and 20 downstream of the injector nozzle exit. The resulting diagramms are depicted in figure 11. For low degrees of superheat of about $R_p \leq 5.5$ the spray angles increase sharply at any distance from the injector exit due to the high-kinetic spray expansion caused by flash boiling. According to [7] this logarithmic growth of the spray angle can be correlated with the number density of bubble clusters, i.e. the nucleation rate. An increase of the nucleation rate generates a higher number of micro bubbles bursting in the liquid jet, which leads to the spray expansion. For higher degrees of superheat the curves become less steep with an asymptotical shape for $R_p \rightarrow \infty$. The nucleation rate is now rather insensitive to the degree of superheat due to volume depletion effects. At the more distant positions of $L/D \geq 10$ the spray angles θ seem to decrease for $R_p > 13$. At these distances the post-processing of the shadowgraphs is limited by the geometrical constraints of the optical access, because the actual spray contour is no longer within the diameter of the window.

DOI: 10.13009/EUCASS2019-418

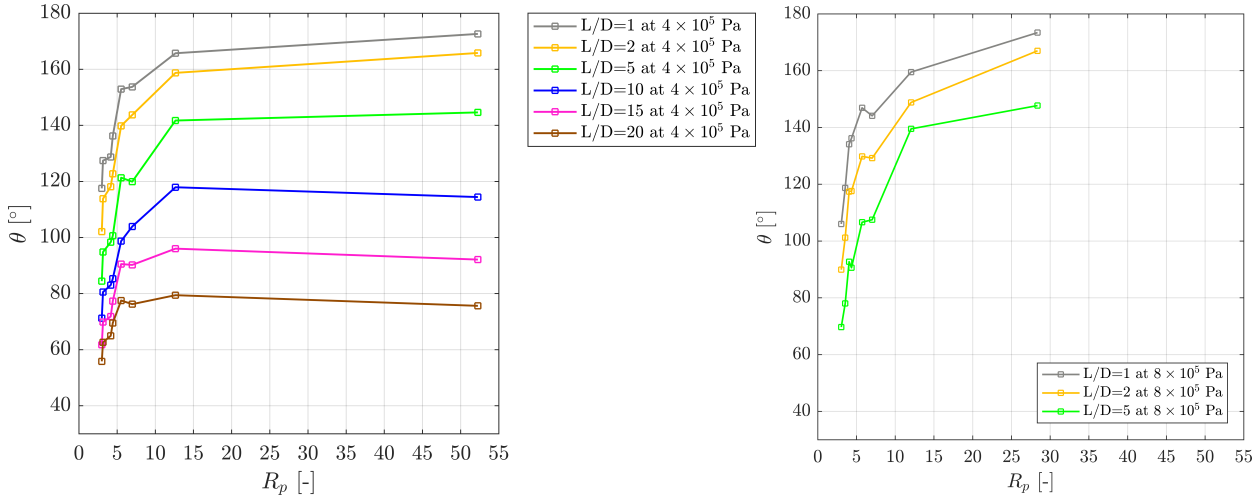

Figure 11: Spray angle θ as a function of the degree of superheat R_p at different locations L/D for $T_{inj} = 82.5$ K, $D_{inj} = 1.0$ mm and $p_{inj} = 4 \times 10^5$ Pa (left) and $p_{inj} = 8 \times 10^5$ Pa (right)

In figure 11 on the left two bends in the diagrams at each L/D-position can be seen. The first bend is at the test runs two and three with superheats of $R_p = 3.2$ and 4.2, respectively, and the second one at the test runs five and six with $R_p = 5.5$ and 7.0. They both coincide with the transition correlations by Cleary et al. [2] in figure 10: The bend at the lower degree of superheat correlates with the lower barrier to an aerodynamical break-up, the one at the higher R_p with the barrier between the transition and the fully flashing regime. The reason for the coincidence of these bends is likely the dependence of the Cleary correlations on the droplet diameter ranges that were used for the definiton of the correlations. But the physical cause for the bends, i.e. for the less steep increase or at distances like $L/D = 5$ even a decrease of the spray angle at these degrees of superheat are currently unknown.

For the test runs with an injection pressure of $p_{inj} = 8 \times 10^5$ Pa the initial spray angle θ at low degrees of superheat is lower compared to the sprays with the injection pressure of $p_{inj} = 4 \times 10^5$ Pa due to the higher mass flow. For the higher injection pressure $p_{inj} = 8 \times 10^5$ Pa only the upper bends corresponding to the upper transition line are visible because none of the test runs with this injection pressure reached the aerodynamical break-up regime, see figures 10 and 11 on the right.

3.2 PDA campaign

After adjusting and aligning the PDA system with the help of a water spray produced by a similar nozzle like the injector nozzle in the CTAIS a first PDA measurement campaign with fully flashing LN2 sprays was performed at a constant position regarding the optical access described in section 2.2.2. The injection temperature was varied in the range of $T_{inj} = 78$ to 96 K for two constant injection pressures $p_{inj} = 4$ and 6×10^5 Pa, respectively. The evolution of the resulting arithmetical mean diameter D_{10} of the droplets is depicted in figure 12. Obviously, the droplet diameter decreases with increasing injection temperature. This is due to the resulting increase of superheat in the liquid, which provides more internal energy for the conversion into kinetic energy during the flash boiling jet break-up. Hence the evaporation and expansion is getting stronger with an increasing injection temperature and smaller droplets are generated. The dependence of the droplet diameter on the injection temperature is less dominant for increasing injection pressures and the droplets are bigger at the same injection temperatures. This is consistent with the results of the shadowgraphy campaign, where the spray angles were smaller for the higher injection pressure at constant degrees of superheat. Another distinctive feature in figure 12 are the mean diameters of the sprays at $p_{inj} = 6 \times 10^5$ Pa for $T_{inj} > 92$ K. Here the droplet diameters are not decreasing further but stay nearly constant similar to the asymptotical trend of the spray angles for an increasing degree of superheat in figure 11.

In figure 13 the arithmetical mean vertical and horizontal velocity components U (left) and V (right) are shown as functions of the injection temperature for the same test runs as above. The results for the vertical velocity component U can be divided in two groups for injection temperatures below $T_{inj} \approx 85$ K and above, respectively. For the first group

DOI: 10.13009/EUCASS2019-418

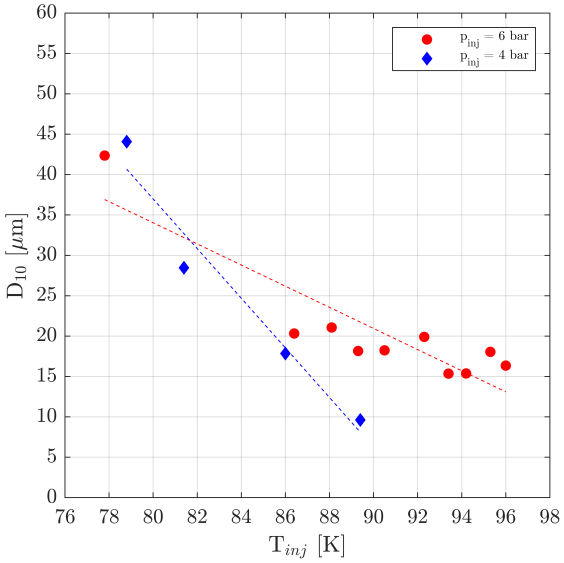

Figure 12: Arithmetical mean diameter D_{10} as a function of the injection temperature T_{inj} at injection pressures of $p_{\text{inj}} = 4$ and 6×10^5 Pa

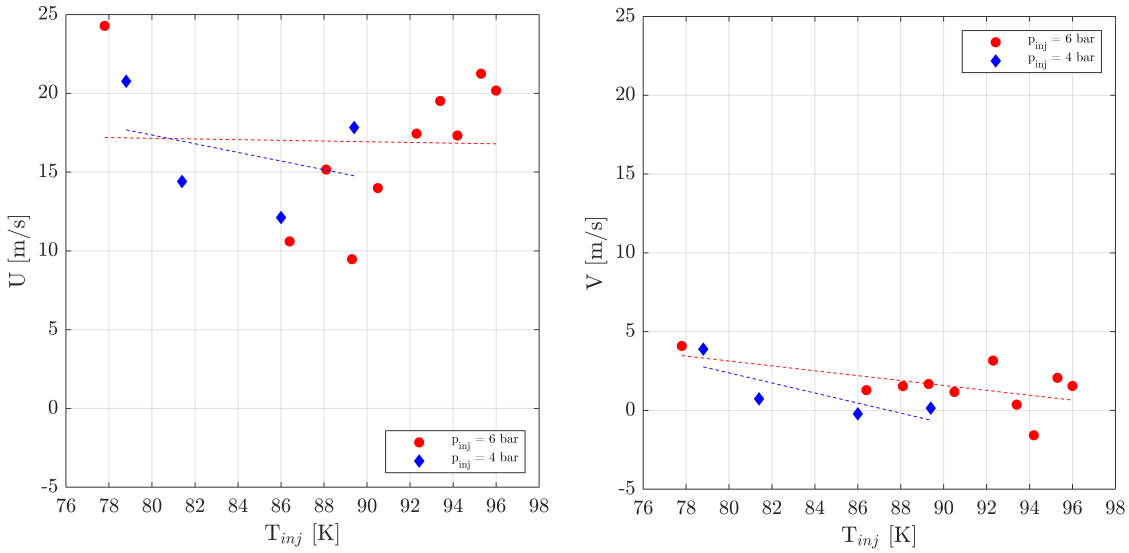

Figure 13: Arithmetical mean vertical and horizontal velocity U (left) and V (right) as a function of the injection temperature T_{inj} at injection pressures of $p_{\text{inj}} = 4$ and 6×10^5 Pa

DOI: 10.13009/EUCASS2019-418

with the lower temperature range the vertical velocities decrease from an initial injection velocity of $u_{\mathrm{inj}} \approx 20\,\frac{\mathrm{m}}{\mathrm{s}}$ until a local minimum is reached around $T_{\mathrm{inj}} \approx 85\,\mathrm{K}$. A further increase of the injection temperature leads to an increase of the vertical velocity. However, in the given temperature range the maximum value of U does not reach the initial injection velocity u_{inj}. The evolution of the horizontal velocity component V is quite flat with a slight decrease for increasing injection temperatures to velocities of $V \approx 0\,\frac{\mathrm{m}}{\mathrm{s}}$. This is due to the measurement position at the spray axis: Small asymmetries appearing in the sprays with low superheats, and therefore with a small influence of flash boiling on the break-up process, are smoothed by the growing dominance of flash boiling with increasing injection temperatures and superheat, respectively.

4. Conclusion and outlook

With the new cryogenic test bench M3.3 with a temperature controlled injection system two measurement campaigns with LN2 were performed. The shadowgraphy campaign showed a clear evolution of the spray morphology with increasing injection temperatures or degrees of superheat, respectively. An increase of the injection pressure dampens this evolution slightly. The results for the cryogenic liquid fit well into correlations developed for storable liquids from literature. The potential of the flash boiling mechanism to generate monodisperse LN2 sprays with high opening angles and small droplets is existing but for the used injection conditions asymptotical limits were reached. The spray angle evolution from the shadowgraphy measurements as well as the diameter and velocity distributions from the PDA campaign both confirm this hypothesis. Especially those distributions together with the well defined injection conditions are helpful and necessary for the development of numerical models about nucleation and bubble growth in superheated cryogenic fluids. This is why the PDA measurements will be intensified and expanded for more positions in the vertical and horizontal direction of the spray axis. To understand the physical reasons for the bends, i.e. less steep increases or even decreases of the spray angle at certain degrees of superheat, more test runs and a more specific data evaluation of the performed tests have to be done. The purpose of all test campaigns with LN2 is not only to provide a detailed data base about flash boiling LN2 sprays for numerical modelling and validation but also to prepare the investigation of flash boiling of the actual rocket propellants like liquid oxygen in the near future or liquid methane later on at this test bench.

5. Acknowledgments

The authors acknowledge funding received from the DFG within the SFB TRR75. The authors thank Johann Fröse, Markus Dengler, Artur Walz-Steinbach and Michael Zepmeisel for their support at the M3.3 test bench before and during the test campaigns. Furthermore the authors thank Marek Czapp and Max Frederik Luh for their assistance with setting up and aligning the PDA system.

References

[1] Aleiferis, P.G., J. Serras-Pereira, A. Augoye, T.J. Davies, R.F. Cracknell, and D. Richardson. Effect of Fuel Temperature on In-Nozzle Cavitation and Spray Formation of Liquid Hydrocarbons and Alcohols from a Real-Size Optical Injector for Direct-Injection Spark-Ignition Engines. *Int. J. Heat Mass Transfer*, 53(21-22):4588–4606, 2010.

[2] Cleary, V., P. Bowen, and H. Witlox. Flashing Liquid Jets and Two-Phase Droplet Dispersion: I. Experiments for Derivation of Droplet Atomisation Correlations. *J. Hazard. Mater.*, 142(3):786–796, April 2007.

[3] De Rosa, M., J. Sender, H. Zimmermann, and M. Oschwald. Cryogenic Spray Ignition at High Altitude Conditions. In *42nd AIAA/ASME/SAE/ASEE JPC*, Sacramento, California, July 2006.

[4] Elias, E. and P.L. Chambré. Flashing Inception in Water During Rapid Decompression. *J. Heat Transfer*, 115(1):231–238, February 1993.

[5] Gemci, T., K. Yakut, N. Chigier, and T.C. Ho. Experimental Study of Flash Atomization of Binary Hydrocarbon Liquids. *Int. J. Multiph. Flow*, 30(4):395–417, 2004.

[6] Johns, H.E. and J.O. Wilhelm. The Refractive Indices of Liquid Oxygen, Nitrogen, and Hydrogen. *Can. J. Res.*, 15(7):101–108, July 1937.

[7] Lamanna, G., H. Kamoun, B. Weigand, C. Manfletti, A. Rees, J. Sender, M. Oschwald, and J. Steelant. Flashing Behavior of Rocket Engine Propellants. *At. Spray*, 25(10):837–856, 2015.

DOI: 10.13009/EUCASS2019-418

[8] Lamanna, G., H. Kamoun, B. Weigand, and J. Steelant. Towards a Unified Treatment of Fully Flashing Sprays. *Int. J. Multiph. Flow*, 58:168–184, 2014.

[9] Luo, M. and O.J. Haidn. Characterization of Flashing Phenomena with Cryogenic Fluid Under Vacuum Conditions. *J. Propul. Power*, 3(5):1253–1263, May 2016.

[10] Manfletti, C. Laser Ignition of an Experimental 400N Cryogenic Reaction and Control Thruster: Pre-Ignition Conditions. *Journal of Propulsion and Power*, 30(4):925–933, July-August 2014.

[11] Meyer, J. Zur Kenntnis des negativen Drucks in Flüssigkeiten. *Abh. Dtsch. Bunsen-Ges. Phys. Chem.*, 3(1):1–53, 1911.

[12] Rees, A., J. Sender, and M. Oschwald. Cryogenic Flash Boiling in Liquid Rocket Engines. In *IICR 5th Cavitation Workshop*, Chania, Crete, June 2017.

[13] Rees, A., J. Sender, and M. Oschwald. Temperature Dependence of Flashing LN2-Jets. In *Space Propulsion Conference*, Seville, Spain, May 2018.

[14] Reitz, R.D. A Photographic Study of Flash-Boiling Atomization. *Aerosol Sci. Technol.*, 12(3):561–569, 1990.

[15] Salzmann, H. and A. Rees. Dokumentation MATLAB-Skript zur Bestimmung des Spraywinkels am Prüfstand M3.3. Technische Beschreibung DLR-LA-RAK-M3.3-TB-002, DLR Lampoldshausen, September 2018.

[16] Senda, J., Y. Hojyo, and H. Fujimoto. Modeling on Atomization and Vaporization Process in Flash Boiling Spray. *JSAE Review*, 15(4):291–296, 1994.

[17] Senda, J., Y. Wada, D. Kawano, and H. Fujimoto. Improvement of Combustion and Emissions in Diesel Engines by Means of Enhanced Mixture Formation Based on Flash Boiling of Mixed Fuel. *Int. J. Engine Res.*, 9(1):15–27, 2008.

[18] Simões-Moreira, J.R., M.M. Vieira, and E. Angelo. Highly Expanded Flashing Liquid Jets. *J. Thermophys. Heat Transfer*, 16(3):415–424, 2002.

[19] Wismer, K.L. The Pressure-Volume Relation of Super-heated Liquids. *J. Phys. Chem.*, 26(4):301–315, June 1921.

[20] Witlox, H., M. Harper, P. Bowen, and V. Cleary. Flashing Liquid Jets and Two-Phase Droplet Dispersion: II. Comparison and Validation of Droplet Size and Rainout Formulations. *J. Hazard. Mater.*, 142(3):797–809, April 2007.

[21] Yildiz, D., P. Rambaud, J. Van Beeck, and J.-M. Buchlin. A Study on the Dynamics of a Flashing Jet. Final Contract Research Report EAR0030, VKI, 2002.

[22] Zeng, Y. and C.-F.F. Lee. An Atomization Model for Flash Boiling Sprays. *Combust. Sci. and Tech.*, 169(1):45–67, 2001.